

# Coaction of intercellular adhesion and cortical tension specifies tissue surface tension

M. Lisa Manning<sup>a</sup>, Ramsey A. Foty<sup>b</sup>, Malcolm S. Steinberg<sup>c</sup>, and Eva-Maria Schoetz<sup>d,1</sup>

<sup>a</sup>Princeton Center for Theoretical Science, Princeton University, Princeton, NJ 08544; <sup>b</sup>University of Medicine and Dentistry of New Jersey-Robert Wood Johnson Medical School, Piscataway, NJ 08854; <sup>c</sup>Department of Molecular Biology, Princeton University, Princeton, NJ 08544; and <sup>d</sup>Lewis-Sigler Institute for Integrative Genomics, Princeton University, Princeton, NJ 08544

Edited\* by Barry H. Honig, Columbia University/Howard Hughes Medical Institute, New York, NY, and approved June 7, 2010 (received for review March 20, 2010)

In the course of animal morphogenesis, large-scale cell movements occur, which involve the rearrangement, mutual spreading, and compartmentalization of cell populations in specific configurations. Morphogenetic cell rearrangements such as cell sorting and mutual tissue spreading have been compared with the behaviors of immiscible liquids, which they closely resemble. Based on this similarity, it has been proposed that tissues behave as liquids and possess a characteristic surface tension, which arises as a collective, macroscopic property of groups of mobile, cohering cells. But how are tissue surface tensions generated? Different theories have been proposed to explain how mesoscopic cell properties such as cell–cell adhesion and contractility of cell interfaces may underlie tissue surface tensions. Although recent work suggests that both may be contributors, an explicit model for the dependence of tissue surface tension on these mesoscopic parameters has been missing. Here we show explicitly that the ratio of adhesion to cortical tension determines tissue surface tension. Our minimal model successfully explains the available experimental data and makes predictions, based on the feedback between mechanical energy and geometry, about the shapes of aggregate surface cells, which we verify experimentally. This model indicates that there is a crossover from adhesion dominated to cortical-tension dominated behavior as a function of the ratio between these two quantities.

differential adhesion hypothesis | differential interfacial tension hypothesis | mathematical modeling | cell aggregate geometry | self-assembly

It is well established that many tissues behave like liquids on long timescales. Cell tracking in vivo and in vitro highlights (*i*) large-scale flows, (*ii*) exchange of nearest neighbors in a cellular aggregate, and (*iii*) rounding-up and fusion of aggregates (1). Macroscopic rheological properties such as surface tension can be measured using a tissue surface tensiometer (TST) (1–8) or micropipette aspiration (9), and surface tension can be used to explain tissue self-organization in embryogenesis (8, 10–12) or cancer (13, 14). In particular, cell sorting and tissue spreading can be explained in terms of tissue surface tensions that differ among cell types (1, 3–5, 8, 15, 16).

A full understanding of tissue surface tension as a driving force for biological processes is important, and knowledge of its cellular origins would allow us to intelligently design drugs and treatments to alter tissue organization. Two opposing theories about the mesoscopic origin of tissue surface tension have coexisted over the last 30 years. One, the differential adhesion hypothesis (DAH), postulates that in analogy to ordinary fluids, tissue surface tension is proportional to the intensity of the adhesive energy between the constituent cells, which are treated as point objects. The DAH has proven successful in a variety of studies with cell lines (2–5, 15), malignant (13, 14) and embryonic tissues (1, 5, 8, 16) and is widely accepted (12, 17). A recent study by Foty and Steinberg (18) experimentally verified a linear relationship between adhesion molecule expression levels and tissue surface tension.

However, recent experiments using atomic force microscopy (AFM) (19) and TST (see data in this study) indicate a dependence of the surface tension on actin-myosin activity in the cell, interpreted as supporting an alternative theory in which cortical tension in individual cells is thought to be the determining factor. The differential interfacial tension hypothesis (DITH) developed by Harris (20), Brodland (21), and Graner (22) relates tissue surface tension to the tension along individual cell interfaces. The DITH theories are appealing because they recognize that individual cells are not point objects; a cell's mechanical energy changes with cell shape and the cortical tension clearly plays a role in this energy balance.

Recent work has emphasized that interfacial tensions arise from a balance of adhesion, cortical tension, and cortical elasticity (17, 19, 23, 24). However, the exact nature of this interplay remains to be elucidated.

In this study, we develop, analytically solve, and experimentally verify a model that specifies an explicit relationship between surface tension and the ratio of adhesion to cortical tension. With this model, we can also explain why the DAH, despite its simplicity, is so successful. Furthermore, we predict regimes where the DAH breaks down and, unlike previous models, show that changes in tissue surface tension must be accompanied by changes in the shapes of surface cells as a function of the ratio between adhesion and cortical tension. In the discussion, we propose future experiments, involving laser ablation and long-time AFM measurement, which could be used to further test the various aspects of our model.

## Results

**Theoretical Description.** We develop a minimal mechanical model based on two experimental systems, zebrafish embryonic tissues and a P-cadherin-transfected L-cell line (LP2). Fig. 1A is a confocal section of a zebrafish aggregate, showing that cells in the bulk are roughly polyhedral with sharp corners, an aspect ratio of unity and without obvious polarization. The rate of cell divisions in zebrafish aggregates is low (1) and cells within a single tissue type are approximately the same size (see Fig. 1A). Our model therefore enforces a constant volume for individual cells,  $V = 1$ , where we have normalized all volumes by the average volume for a single cell.

Because our goal is to understand the collective behavior of cell populations, we can focus on coarse-grained mechanical properties of individual cells such as cortical tension and adhesion. As in other cell models (23, 25, 26), we associate an energy with cell–cell

Author contributions: M.L.M. and E.-M.S. designed research; M.L.M., R.A.F., M.S.S., and E.-M.S. performed research; M.L.M., R.A.F., and E.-M.S. analyzed data; and M.L.M., R.A.F., M.S.S., and E.-M.S. wrote the paper.

The authors declare no conflict of interest.

\*This Direct Submission article had a prearranged editor.

<sup>1</sup>To whom correspondence should be addressed. E-mail: eschoetz@princeton.edu.

This article contains supporting information online at [www.pnas.org/lookup/suppl/doi:10.1073/pnas.1003743107/-DCSupplemental](http://www.pnas.org/lookup/suppl/doi:10.1073/pnas.1003743107/-DCSupplemental).

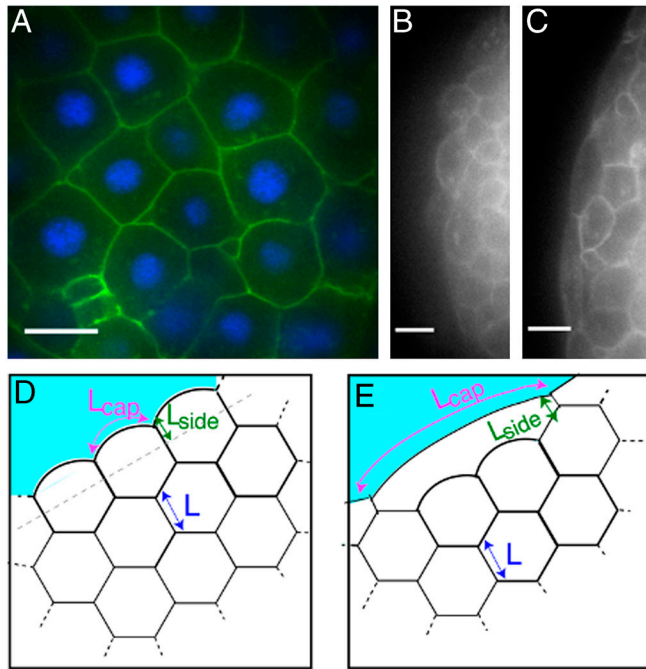


**Fig. 1.** (A–C) Confocal sections of zebrafish aggregates. (Scale bar, 10  $\mu\text{m}$ .) (A) Ectoderm cells in the bulk are densely packed into roughly polyhedral shapes. Membranes are labeled using Gap43-GFP, nuclei using Hoechst. (B) Surface cells in which E-cadherin is down-regulated. Cells have rounded edges and are compact. (C) Surface cells of an ectoderm aggregate. Bulk cells are compact, whereas surface cells are stretched. (D and E) Illustration of ordered packing of cells, where surface cells contact each other over a length  $L_{\text{side}}$ . (D) Cells along the interface with cell–culture medium maintain a compact shape ( $n_{\text{stretch}} = 1$ ). (E) Illustration of stretched surface cells with  $n_{\text{stretch}} = 3$ . This arrangement satisfies force balance and the constant area constraint.

contacts, where the energy is proportional to the surface area of contact between cells:  $W_{\text{ad}} = (\Gamma/2)P_C$ , where  $P_C$  is the surface area (perimeter in 2D) in contact with other cells. In addition, the response of single cells to low-frequency pressures and forces can be characterized by a cortical tension (23, 26, 27):  $W_{\text{cort}} = \beta P_T$  where  $P_T$  is the total surface area of a cell.

Of course, feedbacks between adhesion molecule and cytoskeletal dynamics are abundant, which suggests that the cortical tension along contacting interfaces ( $\beta_C$ ) can be different from that along noncontacting interfaces ( $\beta_{\text{NC}}$ ). Because the cortical-tension energy and adhesive energy both scale linearly with surface area, we can accommodate these feedbacks in a simple way. The term  $\beta = \beta_{\text{NC}}$  is simply the cortical tension of a cell in the absence of any cell–cell contacts, which is the quantity measured in single-cell pipette aspiration experiments (27). We introduce the *effective adhesion*  $\gamma$  which is the total energetic contribution of contacting surfaces. We define this as the difference between the free energy of the adhesive bonds per unit area ( $\Gamma$ ) and local changes to the cortical tension near an interface  $2(\beta_C - \beta_{\text{NC}})$ . Then the coarse-grained mechanical energy for each cell in an aggregate is given by

$$W_{\text{cell}} = (\beta - \gamma/2)P_C + \beta P_{\text{NC}} \quad |V = 1 \quad [1]$$

where  $P_{\text{NC}} = P_T - P_C$  is the surface area of the noncontacting interface. Note that  $(\beta - \gamma/2)$  is half the interfacial tension of cell–cell contacts, and  $\beta$  is the interfacial tension of cell–culture medium interfaces. We observe that cells in the interior of aggregates exhibit polyhedral shapes with sharp corners. As discussed in the *SI Text*, this observation means that when  $\gamma/\beta < 2$ , cortical elasticity must be a small contribution to the energy (at least on the relevant long timescales over which surface tension is a

meaningful quantity). Therefore Eq. 1 neglects elastic terms and is valid when  $\gamma/\beta < 2$ ; we discuss the case  $\gamma/\beta > 2$  in a later section.

Previous methods for approximating tissue surface tension assumed that individual cells do not change their shapes; in this case, the surface tension is simply the difference between the interfacial tensions of cell–cell and cell–culture medium interfaces (21, 26). However, confocal images of the equatorial plane of spherical zebrafish aggregates (Fig. 1B and C) suggest that surface cell shape depends on tissue surface tension, i.e., that there is an interplay between mechanical energy and geometry that must be taken into account. Therefore our strategy will be to find shapes and configurations of cells which locally minimize the mechanical energy and calculate the surface tension of those configurations.

When an aggregate of cells is compressed, the surface area of the aggregate increases, and cells formerly in the bulk are exposed to the surface. Therefore, in exact analogy with fluids, the response of the tissue to changes in surface area is the difference in energy,  $\Delta W$ , between a cell in the bulk and a cell on the surface, multiplied by the number of cells per unit area (or length in 2D) at the surface. The number of cells per unit area is equal to unity divided by the projected area  $A_{\text{proj}}$  (or projected length in 2D) of a single cell onto the surface of the aggregate:

$$\sigma = (W_{\text{surf}} - W_{\text{bulk}})/A_{\text{proj}} \quad [2]$$

In general, this quantity is difficult to calculate for large aggregates because the total energy depends on the exact geometry of each cell in force balance with other cells under the constant volume constraint. However, we have derived an exact solution to this problem for an ordered two-dimensional system.

**Analytical and Numerical Results.** Fig. 1D and E are illustrations of ordered 2D cellular structures with boundaries. Cells in the bulk are hexagonal, all cells have the same fixed area, and individual interfaces must have constant curvature because they are fluid on long timescales and do not support shear stresses. With these constraints, it is possible to parameterize the surface cell shape with only two numbers:  $L_{\text{side}}$ , which is the length of contact surface cells make with other surface cells, and  $n_{\text{stretch}}$ , which is the number of bulk cells that a surface cell stretches across. Fig. 1D illustrates a force-balanced configuration with  $n_{\text{stretch}} = 1$ , and Fig. 1E is a configuration with  $n_{\text{stretch}} = 3$ .

The optimal shape can then be explicitly calculated as the values of  $L_{\text{side}}$  and  $n_{\text{stretch}}$  that minimize Eq. 1. Finally, Eq. 2 is used to calculate the surface tension. We find that  $n_{\text{stretch}} = 1$  always minimizes the energy for  $\gamma/\beta < 2$ , and the surface tension as a function of  $\gamma/\beta$  is given by the dashed line in Fig. 2A and B. There is a generalization of this calculation to ordered structures in three dimensions, which is detailed in the *SI Text*. The surface tension for 3D-ordered aggregates is given by the dashed line in Fig. 2C.

Active processes allow cells to exchange neighbors and explore many possible configurations, so that they are not confined to the global minimum energy configuration. Instead, the collection of cells explores a large number of local minima, and these configurations are disordered, much like the typical configurations of a fluid or a jammed granular material. We use numerical simulations to show that the surface tension for 2D-disordered aggregates is related in a remarkably simple way to that for ordered structures, and make a conjecture about 3D aggregates.

We used the Surface Evolver program developed by Brakke (28) to numerically find the local minimum energy 2D structures for various random initial conditions and values of  $\gamma/\beta$  (see *Methods*). Fig. 2D and E illustrates two minimal structures generated by this procedure: For small values of  $\gamma/\beta$ , surface cells are rounded (Fig. 2D) because they minimize their total perimeter at the expense of cell–cell contacts, whereas, for large values of  $\gamma/\beta$ , cells are flat (Fig. 2E) because they maximize neighbor contacts.



markers as bulk cells (1). Furthermore, they are also indistinguishable in their behavior as surface cells become intermixed with bulk cells during aggregate fusion (1) and cells continue to diffuse in and out of the surface layer (see *SI Text*). We now extend our model to account for these stretched cells and investigate the phenomenon quantitatively in experiments.

**Modeling Stretched Cell Shapes.** When the adhesion is greater than the cortical tension, our mechanical model Eq. 1 predicts that cells will begin to spread out because the line tension is negative,  $dW/dP = -\gamma/2 + \beta < 0$ , so cells will continue to increase their perimeter without limit. This perimeter growth cannot continue unabated because other mechanical forces will eventually cause the cells to stop expanding.

What additional restoring force is consistent with experimental observations? Adhesion molecule regulation generates a plausible restoring force; the amount of energy a single cell can gain by increasing its perimeter must be limited by the number of cadherins on the cell surface, which is itself regulated. Although we do not know the exact form of this regulation, we can expand its energetic contribution as a Taylor series in the difference between the actual adhesive energy and the adhesive energy of a cell with the preferred number of cadherins. Keeping up to second-order terms, this adds a term  $\alpha P_C^2$  to Eq. 1, as discussed in the *SI Text*. Another possible restoring force is elasticity generated by a denser cortical network near cell–cell interfaces; this would also add a term proportional to  $P_C^2$  (22, 24). The remaining analysis does not depend on the mechanistic origin of these forces, but simply requires that the first higher-order term is of the form  $P_C^2$ :

$$W_{\text{cell}} = (\beta - \gamma/2)P_C + \alpha P_C^2 + \beta P_{\text{NC}} \quad |V = 1 \quad [3]$$

The lowest energy states corresponding to this energy functional are complicated because the  $P_C^2$  term introduces a length scale that is not necessarily the same as the length scale introduced by the incompressibility constraint. For example, in two dimensions, the smallest perimeter structure is hexagonal, but the preferred perimeter introduced by the second-order term does not necessarily have to be a hexagon. However, in agreement with experimental observations, a simple assumption is that both length scales are the same and therefore  $\alpha$  increases linearly from zero with  $\gamma/\beta$  for  $\gamma/\beta > 2$ . In this case, the surface cells stretch to make the same contact area as cells in the bulk, and we can calculate the “covering ratio” for ordered 2D packings. Each bulk cell contacts a surface cell over a length  $6L$  and therefore a surface cell covers approximately three bulk cells (see *SI Text*). The calculation for 3D is similar and the projected area of surface cells is 3.7 times greater than that of bulk cells.

**Zebrafish Tissue Surface Cells.** We investigate the covering ratio for the stretched surface cells in disordered 3D zebrafish ectoderm aggregates. We hand-segmented confocal slices as shown in Fig. 4 *A* and *B* from  $n = 15$  aggregates to determine an estimate of the projected areas of each cell. The results are illustrated in Fig. 4*C*. The first observation is that stretched surface cells possess a preferred size that is reproducible from aggregate to aggregate, and there is a significant difference between surface cells and bulk cells. We find that the projected areas are  $226 \pm 100 \mu\text{m}^2$  for the surface cells ( $n_{\text{total}} = 236$ ) and  $62 \pm 9 \mu\text{m}^2$  for the bulk cells ( $n_{\text{total}} = 380$ ), i.e., the ratio between the projected areas is  $3.7 \pm 0.4$ , which is consistent with the theoretical prediction of 3.7. This stretching effect is not due to an increase in volume of surface cells, because using  $V_{\text{cell}} \sim A_{\text{proj}}h$  (where  $h$  is the distance between the cell top and bottom), we find that bulk cells span on average 8–9  $z$  slices and surface cells 3 slices, and  $A_{\text{proj}}$  for surface cells is about 3 times larger than for bulk cells.

What are the theoretical predictions for the surface tension in this case? We use the specific value for  $\alpha$  that makes the contact

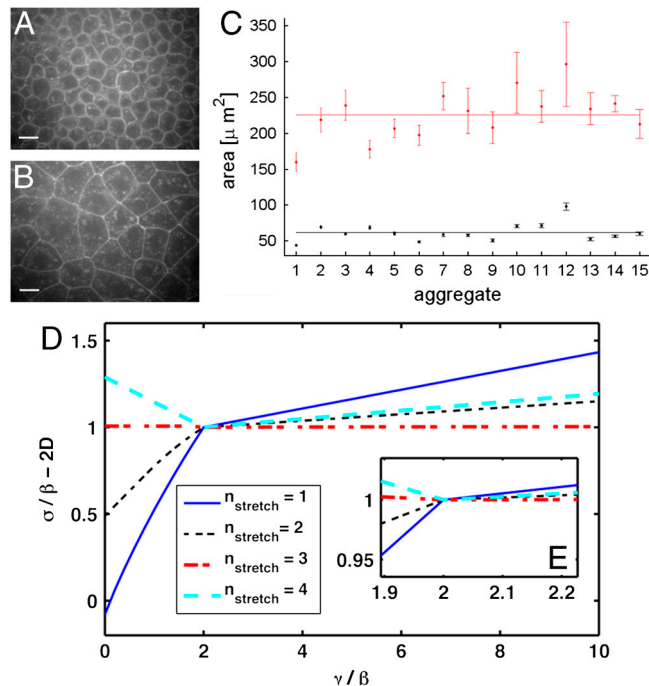


**Fig. 4.** (*A* and *B*) Representative confocal slices of a 3D zebrafish ectoderm aggregate in planes tangent to the aggregate surface. *A* intersects the surface cells, whereas *B* is at a depth of  $>25 \mu\text{m}$  and intersects a layer in the bulk. (Scale bar,  $10 \mu\text{m}$ .) (*C*) Plot of the projected areas of all cells. Red points correspond to surface cells, whereas black points correspond to bulk cells, and the solid lines represent the mean of the entire dataset. Error bars represent errors on the aggregate mean. (*D*) Comparison of the relationship between  $\sigma$ ,  $\gamma$ , and  $\beta$  as obtained from our extended model with  $\alpha = \text{MAX}(0, (\gamma/2 - \beta)/(2P_{\text{hex}}))$ , for various surface cell configurations. The dash-dotted line corresponds to compact cell shapes, whereas the dashed and solid lines correspond to surface cells stretched over two or three cells, respectively. For  $\gamma/\beta < 2$ , compact cell shapes are optimal and the differential adhesion hypothesis is approximately satisfied, whereas for  $\gamma/\beta > 2$ , cells stretched over three interior cells are optimal and cortical tension dominates. (*E*, *Inset*) Magnification of crossover behavior in *D*.

length for bulk and surface cells equal and calculate the surface tension of ordered 2D aggregates for a wide range of values of  $\gamma/\beta$  and  $n_{\text{stretch}}$ . The experimentally observed surface tension and surface cell shape will correspond to the minimum solution at each value of  $\gamma/\beta$ . For  $\gamma/\beta < 2$ , compact surface cell shapes are optimal (solid line in Fig. 4*D*), whereas for  $\gamma/\beta > 2$  the surface cells stretch across three interior cells (dash-dotted line in Fig. 4*D*). The surface tension exhibits a crossover at  $\gamma/\beta \sim 2$  from adhesion-dominated behavior (DAH) to a dependence on the cortical tension and other mechanical effects.

## Discussion

This work has two main implications. The first is that when  $\gamma/\beta < 2$ , surface cells do not stretch out and the differential adhesion hypothesis is essentially correct: Surface cells make fewer adhesive contacts than interior cells and this effect is the primary contribution to the surface tension, just as in fluids. Even though cells change shapes, the surface tension given by the magenta stars in Fig. 2*A* varies almost linearly with the *effective* adhesion. Our framework clarifies that “adhesion” as specified in the DAH must correspond to the net energetic contribution of contacting surfaces, which depends on both the free energy of cadherin binding complexes as well as local changes to the cortical tension induced by those bonds. Furthermore, the balance between cortical tension and adhesion is critical for determining surface cell shapes.

The second implication is that the analogy to fluids breaks down when surface cells stretch to make more nearest neighbor

contacts. In contrast to fluids, if surface cells stretch to have the same net contact perimeter as cells in the bulk, there is no adhesive contribution to the surface tension and the DAH must fail. This observation does not depend on a particular model. We have shown that, in high adhesion zebrafish aggregates, surface cells possess a well-defined, reproducible cross-sectional area that is significantly larger than that for bulk cells. Furthermore, this areal fraction is consistent with the assumption that surface cells are making the same surface area of contact in the bulk. Therefore we do not expect the surface tension of these aggregates to depend strongly on the adhesion.

The observation that stretched surface cells exist also leads us to consider cadherin diffusion. In our model, the adhesive energy density is constant along contacting interfaces, and therefore in stretched cells cadherin molecules must diffuse to the (much larger) contact interface to maintain the same density. However, in compact surface cells extra cadherins do not migrate to the contact interface. As discussed in the *SI Text*, this is a reasonable first approximation because there are no excess cadherins to bind with on the surface of the bulk cells, and therefore compact cells get no energy benefit from such a migration. However, heterogeneities in cadherin density could lead to unique minimum energy cell shapes and investigating these interactions is an avenue for future research.

Can these observed stretched surface cell states be explained by a minimal model? In a regime where adhesion is stronger than cortical tension, we show that stretched surface cells are the minimum energy structures as long as there is a restoring force that regulates the areas of cells in contact. Although there are at least two plausible mechanisms for such a restoring force, adhesion molecule regulation and elasticity of the cortical network, our experiments have not directly tested these assumptions. In addition, when calculating the surface tension shown in Fig. 4D and E, we chose a particular value for the magnitude of this restoring force ( $\alpha$ ) based on the assumption that the contact area preferred by the restoring force is the same as that for bulk cells with sharp corners. If this assumption is relaxed, the surface tension would still exhibit a crossover at  $\gamma/\beta = 2$ , but the exact nature of the crossover would change. Both the existence and the magnitude of the restoring force could be investigated in a future experiment using laser ablation to destroy individual cell–cell interfaces in low and high adhesion aggregates and analyzing the structural relaxation. Farhadifar et al. (23) have suggested that the anisotropy of the network response and the magnitude of the structural relaxation can be used to extract the relative magnitudes of cortical elasticity compared to interfacial tension.

For a model that includes only adhesion and cortical tension (Eq. 1), stretched surface cells are not the minimal energy structures as shown in Fig. 4D and E. Despite this, as  $\gamma/\beta$  approaches two, the energies of stretched states become closer to that for the unstretched states and active processes would allow surface cells to explore these “metastable” configurations. However, we would expect metastable stretched states to have a wide range of projected areas, weighted toward smaller area ratios because these have lower energy. The fact that zebrafish surface cells have a specific, reproducible area fraction significantly greater than unity suggests that these structures are not metastable, but instead have a preferred contact area with other cells as generated by the model described by Eq. 3.

In order to fully interpret the available experimental data in the context of this model, we would like to compare the magnitude of the adhesive tension to that of the cortical tension in individual cells. However, the net effect of adhesive contacts on interfacial tension (which we denote  $\gamma$ ) depends both on the free energy of adhesive molecule bonds and also on changes to the cortical tension along the contacting interface. Therefore it is difficult to determine how changes to the expression levels or activity of cadherins, actin, or myosin affect  $\gamma$ . In a recent study, Foty and Steinberg showed that surface tension increases linearly with

the numbers of surface cadherins (18), in agreement with the DAH and our model if  $\gamma/\beta$  increases linearly with the number of cadherins. However, because the interaction between actin and cadherin-mediated adhesion is a highly dynamic process that is regulated by  $\alpha$ -catenin (29, 30), it is possible to argue that increasing cadherin expression significantly increases cortical tension and  $\gamma/\beta$  remains unknown. Similarly, when we down-regulate surface tension by cytoskeletal drugs, both cortical tension and adhesive energy are decreased because cadherin bonds are stabilized by the cortical network (31–33). One attempt to dissect the connection of cortical tension and adhesion of individual cells was reported by Krieg et al. (19) using AFM measurements. Although in principle AFM is a promising technique for those measurements, thermal drift remains a technical challenge preventing long timescale measurements. The results presented in (19) are on timescales of seconds and therefore too short to be relevant for the interpretation of tissue surface tension, which becomes valid only for long timescales on the order of tens of minutes. At these short timescales, the actin network does not remodel (34, 35) and the AFM probes the cytoskeleton elasticity and not exclusively the cortical tension. In addition, cadherin bonds strengthen significantly over time after initiation, so the adhesion dynamics over long timescales are different from those on short timescales (16, 31, 32).

We propose a set of experiments to evaluate the cortical-tension  $\beta$  and the effective adhesion  $\gamma$ . One possible approach for measuring the cortical tension is micropipette aspiration (27, 33). Also, in the near future it may be possible to reduce AFM drift enough to perform single-cell AFM experiments on the relevant long timescales, allowing one to measure the repulsive force generated by the bare cortical tension. The determination of the effective adhesion  $\gamma$  is more difficult. A semiquantitative approach for studying the effect of  $\gamma/\beta$  would be the use of cell lines that are engineered to express a controlled number of fluorescently labeled adhesion molecules, actin, myosin, and actin-associated proteins as done previously for Madin–Darby canine kidney cells by Yamada and Nelson (36). One could then quantify tissue surface tension and surface cell geometries as a function of the ratio of the densities of these molecules and investigate the predicted crossover in surface cell shapes and energy contributions at  $\gamma/\beta = 2$  in our model. Second, laser ablation experiments can be used to estimate the interfacial tension along cell–cell interfaces (23). Additionally, it would be interesting to adapt the shape-energy functional given by Eq. 1 to a Monte Carlo or Cellular Potts model (26, 37) approach with activated dynamics and compare simulated cell sorting based on this interaction potential with the experimentally available data.

These approaches are an avenue of future research, and for the present our model suggests that surface cell shapes can be used to estimate the ratio between adhesion and cortical tension in an experimental aggregate.

Disordered cellular structures appear in many problems in physics and biology; the fact that one can calculate an analytic expression for their surface energy (Fig. 2A and B) is surprising and useful. For example, Eq. 1 with  $\gamma = \beta$  describes a dry foam and therefore our method can be used to calculate the surface energies of finite 2D foams as a function of cluster size. A simple extension of this work also predicts how cells in the bulk change shape from spheres (when there is no adhesion) to polyhedra with sharp corners when the adhesion is high (see *SI Text*).

We have developed a minimal model that relates tissue surface tension to the mechanical properties of individual cells, such as cortical tension, cell–cell adhesion, and incompressibility. Our model suggests how a crossover from the DAH to significant cortical-tension dependence might occur, which is an important consideration when designing drugs to alter mechanical behavior. Both the DAH and the DITH were developed to explain cell sorting experiments in vitro. Integrating both surface tension-based

hypotheses into a single framework, our model predicts not only that cells sort out according to the surface tension of their aggregates but also that this surface tension exhibits a crossover from a regime where intercellular adhesion is the dominant contributor to one where cortical tension dominates.

## Methods

**Generation of Zebrafish and P-Cadherin Expressing L-Cells Aggregates.** Zebrafish aggregates were generated as previously described in refs. 1 and 5. Mouse embryonic fibroblast L929 cells were cotransfected by electroporation with plasmids encoding P-cadherin and G418 resistance, as previously described (18). Detailed procedures are described in the *SI Text*.

**Fluorescent Microscopy.** For structural studies and antibody staining, zebrafish cell aggregates were imaged on an Olympus spinning disc microscope at room temperature using 10 and 20 $\times$  air or 40 and 60 $\times$  oil objectives. Actin expression was assessed by phalloidin staining (1:100; Invitrogen) and E-cadherin was identified by antibody staining (1:750) (38) as described in ref. 39.

In the *SI Text*, to show the motion of surface cells in and out of the bulk, zebrafish ectoderm aggregates, labeled with histone-conjugated Alexa488, were imaged on a two-photon microscope using a 40 $\times$  water immersion objective. In situ hybridization was carried out as described in refs. 1 and 5, and imaged using a Leica MZ16FA microscope.

**Scanning Electron Microscopy.** Cell aggregates were fixed for 1 h with 2.5% electron microscopy grade glutaraldehyde in 0.15 M cacodylate buffer, pH 7.4, at room temperature. They were washed 3 $\times$  for 10 min with the buffer and dehydrated in a closely graded 50–100% ethanol series stored at 20 $^{\circ}$  for 5-min intervals. They were then transferred through two more changes of ice-cold 100% ethanol for 20 min, washed 2 $\times$  for 10 min with amyl acetate, air dried at room temperature, sputter-coated with gold, and examined in the SEM.

**Determination of Projected Surface Area.** Projected surface areas of surface and bulk cells in cell aggregates were determined using a built-in ImageJ

(version 1.4, National Institutes of Health image) routine. The obtained area pixel counts were imported into Matlab and analyzed as well as plotted. For bulk cells, five neighboring planes, 3  $\mu$ m apart, were compared. We analyzed only cells that were clearly visible in the equatorial plane. The maximum area of each cell was then measured. For surface cells, the problem of not being in the maximum plane does not exist therefore we analyzed only three planes. We concentrated on the surface in the middle of the field of view where the curvature of the aggregate would not significantly distort the cell shapes. We analyzed 15 aggregates from three experimental days and generated a dataset of 236 surface and 380 bulk cells.

**Tissue Surface Tensiometry.** Tissue surface tensiometry was carried out as previously described (1–3, 5). From the force and the shape of the aggregate before and under compression at force equilibrium, tissue surface tension was calculated as described in ref. 1.

**In Silico Generation and Analysis of 2D Cellular Structures.** Standard methods (40, 41) were used to generate a 2D random, soft sphere packing with periodic boundary conditions and a box size  $L$ . A voronoi tessellation of the soft sphere packing was constructed using Matlab, restricted to particles with a center of mass within 0.4L of a randomly chosen point in the packing. This tessellation generates a finite, connected cellular structure composed of  $N$  cells which was then used as an input to the program “Surface Evolver,” by Brakke (28), which numerically minimizes the total perimeter of the entire cellular structure, under the constraint that the area of each cell should equal the average area. Each interior edge of the cell was initialized with a tension unity and each surface edge was initialized with a tension  $(\beta/(2\beta - \gamma))$ . See *SI Text* for additional details.

**ACKNOWLEDGMENTS.** The authors thank J. A. Talbot, S. Thiberge, and the imaging core facility for the two-photon movie, S. F. Norrelykke, W. Ellenbroek, and B. Chen for scientific discussions, and T. Newman and S. F. Norrelykke for reading various versions of the manuscript.

- Schoetz E-M (2008) *Dynamics and Mechanics of Zebrafish Embryonic Tissues—A Study of the Physical Properties of Zebrafish Germ-layer Cells and Tissues and Cell Dynamics During Early Embryogenesis* (Verlag Dr. Mueller Publishing Group, Saarbruecken).
- Foty RA, et al. (1994) Liquid properties of embryonic tissues: Measurement of interfacial tensions. *Phys Rev Lett* 72(14):2298–2301.
- Foty RA, et al. (1996) Surface tensions of embryonic tissues predict their mutual envelopment behavior. *Development* 122(5):1611–1620.
- Forgacs G, et al. (1998) Viscoelastic properties of living embryonic tissues: A quantitative study. *Biophys J* 74(5):2227–2234.
- Schoetz EM, et al. (2008) Quantitative differences in tissue surface tension influence zebrafish germ-layer positioning. *HFSP J* 2(1):1–56.
- Mgharbel A, Delanoë-Ayari H, Rieu J-P (2009) Measuring accurately liquid and tissue surface tension with a compression plate tensiometer. *HFSP J* 3:213–221.
- Norotte C, Marga F, Neagu A, Kosztin I, Forgacs G (2008) Experimental evaluation of apparent tissue surface tension based on the exact solution of the Laplace equation. *Europhys Lett* 81:46003.1–46003.6.
- Davis GS, Phillips HM, Steinberg MS (1997) Germ-layer surface tensions and “tissue affinities” in *Rana pipiens* gastrulae: Quantitative measurements. *Dev Biol* 192:630–644.
- Guevorkian K, Colbert M-J, Durth M, Dufour S, Brochard-Wyart F (2010) Aspiration of biological viscoelastic drops. *Phys Rev Lett* 104(21):218101.
- Armstrong PB (1989) Cell sorting out: The self-assembly of tissues in vitro. *CRC Cr Rev Biochem Mol Biol* 24:119–149.
- Holtfreter J (1944) A study of the mechanics of gastrulation. *J Exp Zool* 95:171–212.
- Steinberg MS (1996) Adhesion in development: An historical overview. *Dev Biol* 180(2):377–388.
- Foty RA, Corbett SA, Schwarzbauer JE, Steinberg MS (1998) Effects of dexamethasone on cadherin-mediated cohesion of human fibrosarcoma HT-1080 cells. *Cancer Res* 58:3586–3589.
- Foty RA, Steinberg MS (1997) Measurement of tumor cell cohesion and suppression of invasion by E- or P-cadherin. *Cancer Res* 57:5033–5036.
- Duguay D, Foty RA, Steinberg MS (2003) Cadherin-mediated cell adhesion and tissue segregation: Qualitative and quantitative determinants. *Dev Biol* 253(2):309–323.
- Borghini N, Nelson JW (2009) Intercellular adhesion in morphogenesis: Molecular and biophysical considerations. *Curr Top Dev Biol* 89(1):1–32.
- Lecuit T, Lenne PF (2007) Cell surface mechanics and the control of cell shape, tissue patterns and morphogenesis. *Nat Rev Mol Cell Biol* 8:633–644.
- Foty RA, Steinberg MS (2005) The differential adhesion hypothesis: A direct evaluation. *Dev Biol* 278(1):255–263.
- Krieg M, et al. (2008) Tensile forces govern germ-layer organization in zebrafish. *Nat Cell Biol* 10(4):429–436.
- Harris AK (1976) Is cell sorting caused by differences in the work of intercellular adhesion? A critique of the Steinberg hypothesis. *J Theor Biol* 61(2):267–285.
- Brodland GW (2003) New information from aggregate compression tests and its implications for theories of cell sorting. *Biorheology* 40:273–277.
- Graner F (1993) Can surface adhesion drive cell-rearrangement? Part I: Biological cell-sorting. *J Theor Biol* 164:455–476.
- Farhadifar R, et al. (2007) The influence of cell mechanics, cell-cell interactions, and proliferation on epithelial packing. *Curr Biol* 17:2095–2104.
- Paluch E, Heisenberg C-P (2009) Biology and physics of cell shape changes in development. *Curr Biol* 19(17):R790–R799.
- Hufnagel L, et al. (2007) On the mechanism of wing size determination in fly development. *Proc Natl Acad Sci USA* 104(10):3835–3840.
- Graner F, Glazier JA (1992) Simulation of biological cell sorting using a two-dimensional extended Potts model. *Phys Rev Lett* 69(13):2013–2016.
- Evans E, Yeung A (1989) Apparent viscosity and cortical tension of blood granulocytes determined by micropipet aspiration. *Biophys J* 56(1):151–160.
- Brakke KA (1992) The surface evolver. *Exp Math* 1(2):141–165.
- Drees F, et al. (2005) [alpha]-Catenin is a molecular switch that binds E-cadherin-[beta]-catenin and regulates actin-filament assembly. *Cell* 123(5):903–915.
- Yamada S, et al. (2005) Deconstructing the cadherin-catenin-actin complex. *Cell* 123(5):889–901.
- Imamura Y, et al. (1999) Functional domains of alpha-catenin required for the strong state of cadherin-based cell adhesion. *J Cell Biol* 144(6):1311–1322.
- McClay DR, Wessel GM, Marchase RB (1981) Intercellular recognition: Quantitation of initial binding events. *Proc Natl Acad Sci USA* 78(8):4975–4979.
- Chu Y-S, et al. (2004) Force measurements in E-cadherin-mediated cell doublets reveal rapid adhesion strengthened by actin cytoskeleton remodeling through Rac and Cdc42. *J Cell Biol* 167(6):1183–1194.
- Adams CL, James Nelson W, Steven J Smith (1996) Quantitative analysis of cadherin-catenin-actin reorganization during development of cell-cell adhesion. *J Cell Biol* 135:1899–1911.
- Angres B, Barth A, Nelson WJ (1996) Mechanism for transition from initial to stable cell-cell adhesion: Kinetic analysis of E-cadherin-mediated adhesion using a quantitative adhesion assay. *J Cell Biol* 134(2):549–557.
- Yamada S, Nelson WJ (2007) Localized zones of Rho and Rac activities drive initiation and expansion of epithelial cell-cell adhesion. *J Cell Biol* 178(3):517–527.
- Mombach JCM, et al. (1995) Quantitative comparison between differential adhesion models and cell sorting in the presence and absence of fluctuations. *Phys Rev Lett* 75(11):2244–2247.
- Babb S, et al. (2001) Zebrafish E-cadherin: Expression during early embryogenesis and regulation during brain development. *Dev Dyn* 221:231–237.
- Köppen M, et al. (2006) Coordinated cell-shape changes control epithelial movement in zebrafish and *Drosophila*. *Development* 133:2671–2681.
- Durian DJ (1997) Bubble-scale model of foam mechanics: Melting, nonlinear behavior, and avalanches. *Phys Rev E* 55:1739–1751.
- O’Hern CS, et al. (2002) Random packings of frictionless particles. *Phys Rev Lett* 88(7):075507.1–075507.4.